Leakage Mitigation in Heterodyne FMCW Radar for Small Drone Detection With Stationary Point Concentration Technique

Junhyeong Park, *Graduate Student Member, IEEE*, Seungwoon Park, Do-Hoon Kim, and Seong-Ook Park, *Senior Member, IEEE*

***Abstract*— To prevent potential hazards posed by fast-evolving drones, it is of importance to develop a radar system for drone detection. Frequency modulated continuous wave (FMCW) radars are widely used for that purpose. Heterodyne architectures are preferred for them to mitigate dc offset errors. Having said that, FMCW radars suffer from permanent leakage from the transmitter into the receiver. The leakage phase noise raises the total noise floor and limits the radar sensitivity. Here, we propose a stationary point concentration (SPC) technique in order to overcome the challenges. The SPC technique concentrates the leakage phase noise on a stationary point to alleviate the impact of the noise. The technique can be realized using digital signal processing without additional hardware. The results show that the proposed technique significantly lowers the noise floor.**

***Index Terms*— Digital signal processing (DSP), down-conversion, frequency modulated continuous wave (FMCW) radar, heterodyne, leakage, noise floor, phase noise, stationary point, stationary point concentration (SPC) technique.**

I. Introduction

THE drone market is growing faster and faster. From aerial videography to delivering packages and even being a new racing sport, drones have a disruptive potential. Since drones are getting smaller, faster, and smarter, however, there has also been a growing concern over the use of them, which could pose an array of threats such as terrorism and crashes. To prevent the potential risks, there is a great need for radar systems that can detect drones, even tiny ones. In response to this demand, many studies on the drone detection have been published recently [1]–[8]. One of the typical radar types for the drone detection is the frequency modulated continuous wave (FMCW) radar [3]–[8]. In comparison with pulse radars, the FMCW radar has the inherent advantages, including lower cost, lower peak power, and higher range resolution. In particular, the major drawback of the pulse radar is in that it has the minimum measuring range since its receiver is turned off while the pulse is being transmitted. In short, pulse radars are blind on short distances [9]. On the other hand, the FMCW radar continuously receives the electromagnetic wave. Therefore, the operational mechanism of the FMCW gives an advantage for the target detection at near distances.

There are two common architectures for the FMCW radar. One is homodyne, and the other is heterodyne. The homodyne FMCW radar directly mixes the reference FMCW signal with received FMCW signals, which results in the baseband beat signals. However, due to the imperfect isolation between the local oscillator (LO) port and the radio frequency (RF) port of the mixer in an RF stage, and between the mixer and the low-noise amplifier (LNA), the self-mixing phenomenon occurs. It produces undesired dc components, which saturate the amplifiers and the analog-to-digital converter (ADC) and corrupt the baseband signal. [10]. On the other hand, the heterodyne FMCW radar suffers much less from dc offsets since beat signals are now generated in the intermediate frequency (IF) stage. The IF stage attenuates the dc offset through a high pass or a bandpass filter. Therefore, the heterodyne FMCW radar has been chosen to take the advantages in many published papers [7], [11]–[14].

Although the heterodyne FMCW radar has many advantages, there are still problems to be addressed regarding an inherent leakage from the transmitter (TX) into the receiver (RX). In the monostatic FMCW radar, the leakage occurs in a circulator due to its inefficient isolation capability, and the mismatch in an antenna also contributes to the leakage [15]–[18]. In the case of bistatic FMCW radars, the transmitted signal is leaked into the receiver by the mutual coupling between the TX and the RX antennas, and their ambient objects also cause the leakage [19]. Because the power of the leakage is much higher than that of the returned signals, the LNA can be saturated [15], [19]. In addition, the phase noise of the leakage limits the dynamic range of FMCW radars [15], [18].

Manuscript received September 14, 2018; revised November 15, 2018; accepted November 20, 2018. Date of publication January 8, 2019; date of current version March 5, 2019. This work was supported in part by the UAV Safety Technology Research Program funded by the Ministry of Land, Infrastructure and Transport of Korean Government under Grant 18ATRP-C108186-04 and in part by the Institute for Information and communications Technology Promotion grant funded by the Korea Government (MSIT) under Grant 2018-0-01658, Key Technologies Development for Next Generation Satellites. (*Corresponding author: Junhyeong Park.)*

The authors are with the School of Electrical Engineering, Korea Advanced Institute of Science and Technology, Daejeon 34141, South Korea (e-mail: bdsfh0820@kaist.ac.kr; physicsoly@kaist.ac.kr; dohoonh@kaist.ac.kr; soparky@kaist.ac.kr).

Color versions of one or more of the figures in this paper are available online at http://ieeexplore.ieee.org.

Digital Object Identifier 10.1109/TMTT.2018.2889045

The most important and basic goal is to increase the signal-to-noise ratio (SNR) for detecting small drones, which can be done by mitigating the leakage. There have been many studies to attenuate the leakage. In [7] and [11], there were attempts to reduce the leakage by putting the TX apart from the RX. To increase the distance between the TX and the RX, 106.2-m fiber-optic cables that have low-loss characteristics were used in [7]. In the case of [11], 75-Ω coaxial cables whose lengths are 10 m for the TX and 30 m for the RX were used. In [16], adding a closed loop leakage canceller for the monostatic radar was proposed. The closed-loop leakage canceller adaptively generates an error vector including the amplitude and phase information of the leakage. In [15], [17], and [18], the scheme in [16] was realized using digital signal processing (DSP) and was improved by up-converting the error signal to a preselected reference frequency to avoid the dc offset. In [20], a balanced topology that uses Lange couplers and a Wilkinson combiner was introduced in the radar front-end to cancel out the leakage. In [21], more advanced topology than [20] was suggested, and another topology called as a quadrature radar topology was proposed in [22]. In [23]–[27], various advanced heterodyne architectures were proposed and attempted to solve the problem using a hardware approach. In [28]–[31], the reflections caused by fixed objects in front of the antennas were studied. They expressed these reflections as a short-range (SR) leakage. Based on the correlation statistics of the decorrelated phase noise (DPN), delay time can be selected, which was realized by adding an artificial on-chip target in the RF stage. Then, after mixing expected parameters in the digital IF stage, the sampled IF signal that is similar to the sampled IF signal of the SR leakage was generated. The SR leakage was canceled by subtracting the two IF signals.

In [32], we proposed a new down-conversion concept to mitigate the leakage. However, because the hardware system was not complete at that time, there were only simple simulation results, which are not enough to demonstrate the actual effectiveness of the proposed concept. In addition, more analyses based on both the theories and simulations to verify the proposed concept were required. In this paper, we provide detailed analyses on the proposed theory with the simulations. We also introduce detailed procedures to realize the proposed concept in practice. We present the simulation results and the experiment results to demonstrate the performance of the proposed technique.

So far, the trend in the field on the leakage of the FMCW radar has been to cancel out the leakage by trying to create the same signal with the leakage and subtract it from the received signal [15]–[18], [20]–[22], [25], [27]–[31]. Out of this trend, the proposed concept suggests a novel approach to significantly mitigate the leakage. The proposed concept extracts the frequency and the constant phase information of the leakage beat signal in the digital IF domain. After generating the digital numerically controlled oscillator (NCO) that has the extracted frequency and constant phase values of the leakage beat signal, the received signal is finally down-converted with the digital NCO as a LO signal of the last stage does. By doing this, the frequency and the constant phase in the leakage beat signal are removed, which means the phase noise of the leakage is concentrated on the stationary point. Also, the major phase noise term of the leakage beat signal equation is eliminated. Therefore, the magnitude of the phase noise of the leakage is significantly attenuated, and the noise floor is decreased.

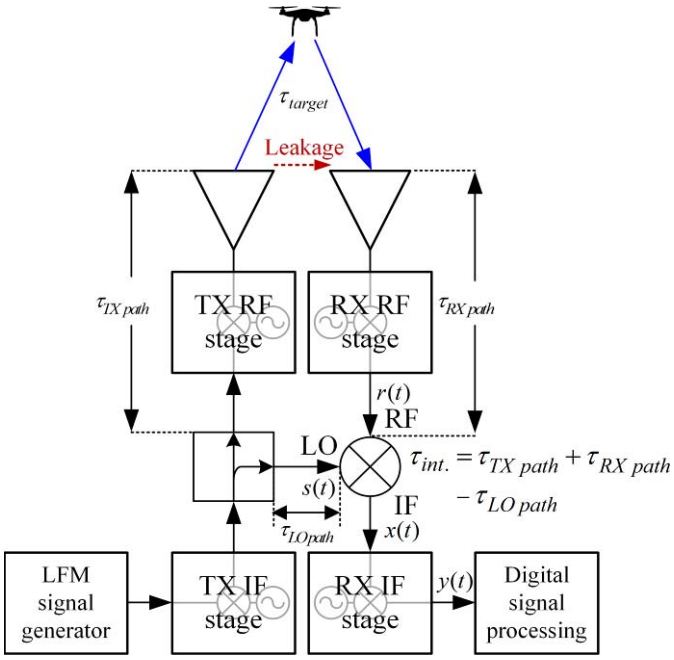

Fig. 1. Block diagram of heterodyne FMCW radar.

Unlike the existing techniques [7], [11], [15]–[18], [20]–[31], the proposed technique can be realized using DSP without additional hardware parts. Also, relatively simple and understandable heterodyne hardware system can be used. In order to emphasize the key of the proposed technique, we named it a stationary point concentration (SPC) technique. We present the results of two experiments to verify the technique. The first experiment shows how much the noise floor is decreased when the leakage only exists without any targets. The second experiment, with the small drones, DJI Inspire I and DJI Spark, verifies the increased SNR. MATLAB R2017a is used for all DSPs in the simulations and the experiments.

In Section II, the theories of the heterodyne FMCW radar and the proposed SPC technique are introduced. In Section III, detailed procedures of the SPC technique are explained. In Section IV, simulation analyses on the SPC technique are shown. Then, in Section V, the FMCW radar used for the experiments is explained. Section VI describes two experiments for the verification and gives the experiment results and the discussion. Our conclusions are drawn in Section VII.

II. Theories

A. Heterodyne FMCW Radar

Fig. 1 shows a block diagram of the heterodyne FMCW radar. A linear frequency modulated (LFM) signal, which is also called a ramp signal or chirp signal is divided into two paths by a splitter. One passes the TX RF stage including cables, LO, mixers, filters, isolators, power amplifiers, and

so on. The LFM signal is then up-converted and radiated by the TX antenna. The other LFM signal, which is called the reference LFM signal, is mixed with the received LFM signals. Due to the FMCW mixing, the beat signals that include the distance and even Doppler information of targets are extracted.

In Fig. 1, the reference LFM signal at the LO port, $s(t)$, can be defined as follows:

$$s(t) = A_S \cos(2\pi f_{TX} t + \pi \alpha t^2 + \theta_S + \varphi_S(t)) \tag{1}$$

for $0 < t < T$, where A_S and f_{TX} are the amplitude and the start frequency of the reference LFM signal. $\alpha = \mathrm{BW}/T$ is the slope of the chirp. BW and T are the sweep bandwidth and the sweep period. θ_S and $\varphi_S(t)$ are the constant phase and the phase noise of the reference LFM signal. The delay from the splitter to the mixer for the FMCW mixing, i.e., $\tau_{\mathrm{LO\ path}}$, is calculated with the other delays at the RF port.

After passing the TX RF stage, the LFM signal is delayed by $\tau_{\mathrm{TX\ path}}$. After transmitted from the TX antenna, the leaked LFM signal directly enters the RX antenna. Then, the signals reflected by targets follow. After received by the RX antenna, these signals pass the RX RF stage including LNAs, isolators, LO mixers, filters, cables, and so on. An another internal delay, $\tau_{\mathrm{RX\ path}}$, is therefore added. In this paper, only the dominant leakage is considered. We assume that the time delay due to the spatial path between the antennas is negligible for the quasi-monostatic radar. Therefore, the received signals at the RF port, $r(t)$, can be expressed as follows:

$$\begin{aligned} r(t) = {} & \underbrace{A_L \cos(2\pi f_{\mathrm{RX}}(t-\tau_{\mathrm{int.}}) + \pi\alpha(t-\tau_{\mathrm{int.}})^2 + \theta_R + \varphi_L(t))}_{\text{Leakage}} \\ & + \underbrace{\sum_{k=1}^{K} A_{T,k} \cos(2\pi f_{\mathrm{RX}}(t-\tau_{\mathrm{int.}}-\tau_{T,k}) \\ & \qquad + \pi\alpha(t-\tau_{\mathrm{int.}}-\tau_{T,k})^2 + \theta_R + \varphi_{T,k}(t))}_{\text{Targets}} \end{aligned} \tag{2}$$

where θ_R is the constant phase of the received LFM signals, A_L and $A_{T,k}$ and $\varphi_L(t)$ and $\varphi_{T,k}(t)$ are the amplitudes and the phase noises of the leakage and the target LFM signals at the RF port. f_{RX} is the start frequency at the RF port. $\tau_{\mathrm{int.}}$ is the total internal delay, $\tau_{\mathrm{int.}} = \tau_{\mathrm{TX\ path}} + \tau_{\mathrm{RX\ path}} - \tau_{\mathrm{LO\ path}}$. $\tau_{T,k}$ is the round-trip delay to targets.

In the heterodyne architecture, there are LO signals in the TX RF stage and the RX RF stage for the up-conversion and the down-conversion. These LO signals have their own phase noises, $\varphi_{\mathrm{TX\ RF\ LO}}(t)$ and $\varphi_{\mathrm{RX\ RF\ LO}}(t)$, which are different from those of the LFM signals, because voltage-controlled oscillators in phase-locked loops for the LO signals are independent. $\varphi_L(t)$ and $\varphi_{T,k}(t)$ can be represented as follows:

$$\begin{aligned} \varphi_L(t) \approx {} & \varphi_S(t-\tau_{\mathrm{int.}}) + \varphi_{\mathrm{TX\ RF\ LO}}(t-\tau_{\mathrm{TX\ path}}-\tau_{\mathrm{RX\ path}}) \\ & - \varphi_{\mathrm{RX\ RF\ LO}}(t-\tau_{\mathrm{RX\ path}}) \end{aligned} \tag{3}$$

$$\begin{aligned} \varphi_{T,k}(t) \approx {} & \varphi_S(t-\tau_{\mathrm{int.}}-\tau_{T,k}) \\ & + \varphi_{\mathrm{TX\ RF\ LO}}(t-\tau_{\mathrm{TX\ path}}-\tau_{\mathrm{RX\ path}}-\tau_{T,k}) \\ & - \varphi_{\mathrm{RX\ RF\ LO}}(t-\tau_{\mathrm{RX\ path}}-\tau_{T,k}). \end{aligned} \tag{4}$$

Finally, after the FMCW mixing, the desired terms that are IF beat signals, $x(t)$, can be written as

$$\begin{aligned} & x(t) \\ & = x_{\mathrm{IF\ leakage}}(t) + x_{\mathrm{IF\ targets}}(t) \\ & = \frac{A_S A_L}{2} \cos\Bigg(2\pi\Big(\overbrace{\underbrace{f_{\mathrm{TX}} - f_{\mathrm{RX}}}_{f_{\mathrm{IF\ carrier}}} + \underbrace{\alpha\tau_{\mathrm{int.}}}_{f_{\mathrm{beat\ leakage}}}}^{f_{\mathrm{IF\ beat\ leakage}}}\Big)t \\ & \qquad + \underbrace{\theta_S + 2\pi f_{\mathrm{RX}}\tau_{\mathrm{int.}} - \pi\alpha\tau_{\mathrm{int.}}^2 - \theta_R}_{\theta_{\mathrm{IF\ leakage}}} + \varphi_{\mathrm{IF\ leakage}}(t)\Bigg) \\ & \quad + \sum_{k=1}^{K} \frac{A_S A_{T,k}}{2} \\ & \quad \times \cos\Bigg(2\pi\Big(\overbrace{\overbrace{\underbrace{f_{\mathrm{TX}} - f_{\mathrm{RX}}}_{f_{\mathrm{IF\ carrier}}} + \underbrace{\alpha\tau_{\mathrm{int.}}}_{f_{\mathrm{beat\ leakage}}}}^{f_{\mathrm{IF\ beat\ leakage}}} + \underbrace{\alpha\tau_{T,k}}_{f_{\mathrm{beat\ targets},k}}}^{f_{\mathrm{IF\ beat\ targets},k}}\Big)t \\ & \qquad + \underbrace{\theta_S + 2\pi f_{RX}(\tau_{\mathrm{int.}} + \tau_{T,k}) - \pi\alpha(\tau_{\mathrm{int.}} + \tau_{T,k})^2 - \theta_R}_{\theta_{\mathrm{IF\ targets},k}} \\ & \qquad + \varphi_{\mathrm{IF\ targets},k}(t)\Bigg). \end{aligned} \tag{5}$$

The phase noises of the IF beat signals of the leakage and targets, $\varphi_{\mathrm{IF\ leakage}}(t)$ and $\varphi_{\mathrm{IF\ targets,k}}(t)$, are

$$\begin{aligned} \varphi_{\mathrm{IF\ leakage}}(t) = {} & \underbrace{\varphi_S(t) - \varphi_S(t-\tau_{\mathrm{int.}})}_{\mathrm{DPN}} \\ & - \varphi_{\mathrm{TX\ RF\ LO}}(t-\tau_{\mathrm{TX\ path}}-\tau_{\mathrm{RX\ path}}) \\ & + \varphi_{\mathrm{RX\ RF\ LO}}(t-\tau_{\mathrm{RX\ path}}) \end{aligned} \tag{6}$$

$$\begin{aligned} \varphi_{\mathrm{IF\ targets},k}(t) = {} & \underbrace{\varphi_S(t) - \varphi_S(t-\tau_{\mathrm{int.}}-\tau_{T,k})}_{\mathrm{DPN}} \\ & - \varphi_{\mathrm{TX\ RF\ LO}}(t-\tau_{\mathrm{TX\ path}}-\tau_{\mathrm{RX\ path}}-\tau_{T,k}) \\ & + \varphi_{\mathrm{RX\ RF\ LO}}(t-\tau_{\mathrm{RX\ path}}-\tau_{T,k}). \end{aligned} \tag{7}$$

In (5), we assume $f_{\mathrm{TX}} > f_{\mathrm{RX}}$ so that the beat frequency is added to the IF carrier frequency, $\mathrm{f_{IF\ carrier}}$. If $f_{\mathrm{TX}} < f_{\mathrm{RX}}$, the beat frequency is subtracted from the IF carrier frequency, $|f_{\mathrm{TX}} - f_{\mathrm{RX}}|$. Also, note that the beat frequency of the leakage, $f_{\mathrm{beat\ leakage}}$, comes from the total internal delay, $\tau_{\mathrm{int.}}$.

In (6) and (7), there are many phase noise terms. The total phase noises follow the largest phase noise, which are described by the power spectral density (PSD). The terms, $\varphi_S(t) - \varphi_S(t-\tau_{\mathrm{int.}})$ and $\varphi_S(t) - \varphi_S(t-\tau_{\mathrm{int.}}-\tau_{T,k})$, which are also called DPN, have the range correlation effect [28]–[31], [33]. Because the range correlation effect reduces the magnitude of $\varphi_S(t)$ [28], [33], the phase noises of the LOs in the RF stages are dominant over the DPN terms.

After the IF beat signals pass the RX IF stage, they are finally down-converted to get rid of the IF carrier frequency.

Only the beat signals are extracted. The IF carrier frequency, $f_{\text{IF carrier}} = f_{\text{TX}} - f_{\text{RX}}$, is decided by a prior frequency planning. Thus, f_μ is chosen as the frequency of the last LO, that is

$$\text{LO}_{\text{common}}(t) = A_{\text{LO}} \cos(2\pi f_{\text{IF carrier}} t + \theta_{\text{LO}} + \varphi_{\text{LO}}(t)) \quad (8)$$

where A_{LO}, θ_{LO}, and $\varphi_{\text{LO}}(t)$ are the amplitude, the constant phase, and the phase noise of the last LO, respectively. If (5) is mixed with (8) and passes a low-pass filter (LPF), then the final signal, $y(t)$, can be represented as follows:

$$\begin{aligned} y(t) &= y_{\text{leakage}}(t) + y_{\text{targets}}(t) \\ &= \underbrace{A_{\text{leakage}} \cos(2\pi f_{\text{beat leakage}} t + \theta_{\text{leakage}} + \varphi_{\text{leakage}}(t))}_{\text{Leakage}} \\ &\quad + \underbrace{\sum_{k=1}^{K} A_{\text{targets},k} \cos(2\pi (f_{\text{beat leakage}} + f_{\text{beat targets},k}) t + \theta_{\text{targets},k} + \varphi_{\text{targets},k}(t)).}_{\text{Targets}} \end{aligned} \quad (9)$$

In (9), $A_{\text{leakage}} = A_S A_L A_{LO}/4$, $A_{\text{targets},k} = A_S A_{T,k} A_{LO}/4$, $\theta_{\text{leakage}} = \theta_{\text{IF leakage}} - \theta_{LO}$, $\theta_{\text{targets},k} = \theta_{\text{IF targets},k} - \theta_{\text{LO}}$, $\varphi_{\text{leakage}}(t) = \varphi_{\text{IF leakage}}(t) - \varphi_{\text{LO}}(t)$, and $\varphi_{\text{targets,k}}(t) = \varphi_{\text{IF targets,k}}(t) - \varphi_{\text{LO}}(t)$. Then, according to the cosine sum identity, $y_{\text{leakage}}(t)$ in (9) can be transformed as follows:

$$\begin{aligned} &y_{\text{leakage}}(t) \\ &= A_{\text{leakage}} \cos(2\pi f_{\text{beat leakage}} t + \theta_{\text{leakage}}) \cos(\varphi_{\text{leakage}}(t)) \\ &\quad - A_{\text{leakage}} \sin(2\pi f_{\text{beat leakage}} t + \theta_{\text{leakage}}) \sin(\varphi_{\text{leakage}}(t)). \end{aligned} \quad (10)$$

Since in general the phase noise is much smaller than 1 [28], [33], [34], (10) can be approximated as follows:

$$\begin{aligned} &y_{\text{leakage}}(t) \\ &\approx A_{\text{leakage}} \cos(2\pi f_{\text{beat leakage}} t + \theta_{\text{leakage}}) \\ &\quad - \underbrace{A_{\text{leakage}} \varphi_{\text{leakage}}(t) \sin(2\pi f_{\text{beat leakage}} t + \theta_{\text{leakage}})}_{\text{Major cause of the noise floor rise}}. \end{aligned} \quad (11)$$

As expressed in (11), the phase noise of the leakage beat signal is up-converted to $f_{\text{beat leakage}}$. It manifests itself as voltage or current noise. Also, A_{leakage} is generally much larger than $A_{\text{targets},k}$ [15], [19]. These properties result in the strong leakage beat signal in the power spectrum, which increases the overall noise floor.

B. Stationary Point Concentration Technique

The proposed SPC technique is applied after the FMCW mixing. When finally down-converted, the SPC technique uses the exact IF beat frequency of the leakage, $f_{\text{IF beat leakage}} = f_{\text{IF carrier}} + f_{\text{beat leakage}}$, and the exact IF constant phase of the leakage, $\theta_{\text{IF leakage}}$ for the last LO, whereas the common method just uses the known IF carrier frequency, $f_{\text{IF carrier}}$. In other words, we propose the following LO:

$$\begin{aligned} \text{LO}_{\text{proposed}}(t) = A_{\text{LO}} \cos(2\pi f_{\text{IF beat leakage}} t + \theta_{\text{IF leakage}} \\ + \varphi_{\text{LO}}(t)). \end{aligned} \quad (12)$$

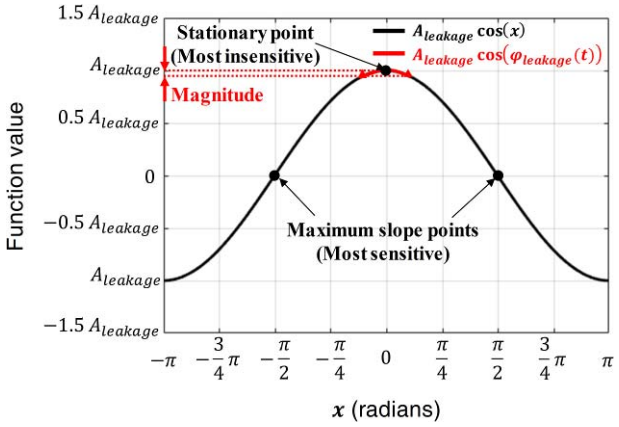

Fig. 2. Phase noise of leakage on stationary point.

If (5) is mixed with (12) and passes the LPF, then the final signal, $z(t)$, as a result of the proposed SPC technique, can be expressed as follows:

$$\begin{aligned} z(t) &= \underbrace{A_{\text{leakage}} \cos(\varphi_{\text{leakage}}(t))}_{\text{Leakage}} \\ &\quad + \underbrace{\sum_{k=1}^{K} A_{\text{targets},k} \cos\left(2\pi f_{\text{beat targets},k}\, t + \theta'_{\text{targets},k} + \varphi_{\text{targets},k}(t)\right)}_{\text{Targets}} \end{aligned} \quad (13)$$

where $\theta'_{\text{targets},k} = \theta_{\text{IF targets},k} - \theta_{\text{IF leakage}}$.

In (13), now that the leakage beat signal does not have any frequency and any constant phase, the term of the major cause of the noise floor rise in (11) is removed. The only term associated with the phase noise of the leakage is the term that envelopes the phase noise of the leakage of the cosine function in (13). This term can be approximated to A_{leakage}, if the same approximation in (11) is applied. Then the leakage is represented as merely a dc value. Therefore, the proposed technique can be an effective solution of the phase noise of the leakage.

Even if we do not use the approximation, the overall effects of the proposed technique can be explained by Fig. 2. Using the SPC technique the phase noise of the leakage is concentrated on the stationary point of the cosine function, because the leakage beat signal does not have frequency and constant phase. In case of the common method, the leakage beat signal, $y_{\text{leakage}}(t)$, has the beat frequency, thus the phase noise of the leakage can tremble at every point including the maximum slope points on the cosine function. On the other hand, in case of the SPC technique, the phase noise of the leakage trembles only at the stationary point. Therefore, the magnitude of the phase noise significantly decreases, which results in the mitigation of the leakage.

In addition, thanks to the SPC technique, the beat frequency of the leakage, $f_{\text{beat leakage}}$, caused by the total internal delay, $\tau_{\text{int.}}$, is removed in the target beat signals. The distance information of targets therefore becomes more accurate. Although the constant phases of the target beat signals are changed due

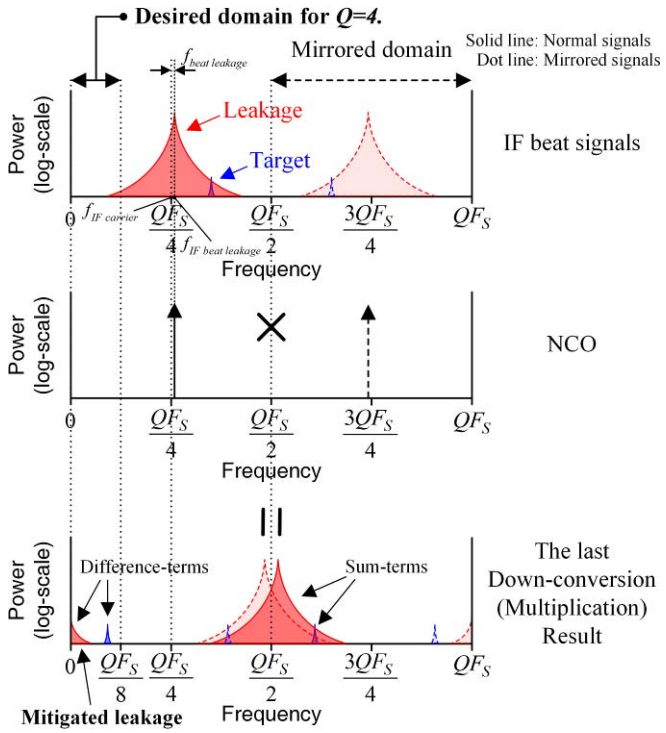

Fig. 3. Results of last down-conversion using SPC technique when the proposed strategic frequency planning and oversampling are applied.

to the SPC technique, its influence on those powers of the signals is insignificant.

III. Realization of Stationary Point Concentration Technique

A. Strategic Frequency Planning and Oversampling

The SPC technique is realized using the DSP. After generating the digital NCO whose frequency and constant phase are same as those of the IF beat signal of the leakage, then it is multiplied with the IF beat signals at the last down-conversion. Importantly, the sampling and the frequency planning for the IF beat signals should be considered carefully. Once the digital bandwidth is set, twice the bandwidth is the minimum available sampling frequency by the Nyquist theorem. However, if the multiplication is carried out for the IF beat signals sampled by this sampling frequency, the undesired sum-terms or their mirrored terms are included in the desired frequency domain.

Therefore, the frequency planning and the sampling are important. The strategic frequency planning and oversampling proposed for the SPC technique are depicted in Fig. 3. The IF beat frequency of the leakage, $f_{\text{IF beat leakage}}$, is placed around a quarter point of the oversampled frequency domain. In this way, we can keep the desired domain as far away as possible from the sum-terms and their mirrored terms. Also, these undesired terms are disposed around the center of the digital IF frequency domain, which means that the sum-terms now can be easily removed by a digital LPF.

As the oversampling factor that is a positive rational number, Q, is increased, the sum-terms and their mirrored terms are pushed further away from the desired domain, preventing any harmful influences. However, if Q is too large, the cost of the ADC rises due to the high sampling rate. Small Q also gives a trouble. For example, if Q is 2, it can encounter the aliasing of the sum-terms. Therefore, it is required to determine the appropriate oversampling factor considering the engineer's own designs.

It is difficult to predict $f_{\text{beat leakage}}$ before manufacturing the FMCW radar. However, $f_{\text{IF beat leakage}}$ is mostly governed by $f_{\text{IF carrier}}$ because $f_{\text{IF carrier}}$ is usually much larger than $f_{\text{beat leakage}}$. Thus, the strategic frequency planning that places $f_{\text{IF carrier}}$ instead of $f_{\text{IF beat leakage}}$ on a quarter point of the oversampled frequency domain is preferable. Fig. 3 reflects the above explanations. $f_{\text{IF carrier}}$ is $QF_S/4$. The IF beat signal of the leakage whose frequency is $f_{\text{IF beat leakage}}$ slightly misses $QF_S/4$ point. Nevertheless, the sum-terms are around the center of the oversampled frequency domain, so the digital LPF can remove these easily. Even in special cases when a long internal delay, large $f_{\text{beat leakage}}$, is inevitable [7], [11], the proposed technique also can be applied by increasing Q.

When we consider the undersampling which is also called the bandpass sampling, the strategic frequency planning proposed can be realized on other frequencies, $QF_S(4N+1)/4$, where N is a natural number.

B. Last Down-Conversion With Digital NCO

A block diagram of the SPC technique is shown in Fig. 4. The oversampled IF beat signal, $x[n]$, can be written as follows:

$$\begin{aligned} x[n] &= \frac{A_S A_L}{2}\cos\left(2\pi f_{\text{IF beat leakage}} n\frac{T_S}{Q} + \theta_{\text{IF leakage}} + \varphi_{\text{IF leakage}}\left(n\frac{T_S}{Q}\right)\right) \\ &\quad + \sum_{k=1}^{K}\frac{A_S A_{T,k}}{2}\cos\left(2\pi\left(f_{\text{IF beat leakage}} + f_{\text{beat targets},k}\right)n\frac{T_S}{Q} + \theta_{\text{IF targets},k} + \varphi_{\text{IF targets, k}}\left(n\frac{T_S}{Q}\right)\right) \end{aligned} \tag{14}$$

where $T_S/Q = 1/QF_S$ is the oversampling interval. The large power of the leakage signal is a general obstacle. However, we change this to a solution for finding out the values of $f_{\text{IF beat leakage}}$ and $\theta_{\text{IF leakage}}$. We use the fact that the magnitude of the leakage beat signal is much larger than that of the target beat signal [15], [19]. After applying the fast Fourier transform (FFT) to $x[n]$, we transform the FFT results to the power spectrum and the phase response. When the FFT is applied, we use the zero-padding to minimize the error caused by insufficient spacing in the frequency domain. Results of the FFT with the zero-padding converge to those of the discrete time Fourier transform. This proves that the zero-padding helps find the real location of the signal peak [35], [36]. Using this advantage of the zero-padding, we can find out the peak that represents the maximum power around a quarter point of the oversampled frequency domain. By doing so,

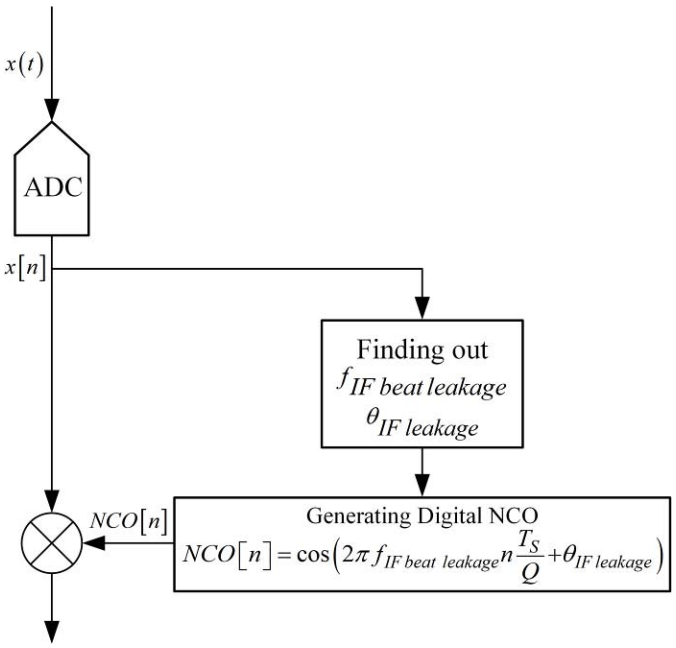

Fig. 4. Block diagram of SPC technique.

the index number, $k_{\text{IF leakage}}$, from the maximum peak can be extracted. Finally, we can find out $f_{\text{IF beat leakage}}$ and $\theta_{\text{IF leakage}}$ as follows:

$$\begin{aligned} k_{\text{IF leakage}} &= \underset{\frac{QF_S}{4}<k<\frac{QF_S}{2}}{\arg\max} |X[k]|^2 \\ f_{\text{IF beat leakage}} &= \frac{\text{QF}_\text{S}}{\text{NFFT}}[k_{\text{IF leakage}} - 1] \\ \theta_{\text{IF leakage}} &= \angle X[k_{\text{IF leakage}}] \end{aligned} \tag{15}$$

where $X[k]$ is the result of NFFT-point FFT of $x[n]$, NFFT is the total number of real samples and zero-pads, QF_S is the sampling frequency for the oversampling, and $\angle X$ is the phase response of $X[k]$.

With the extracted $f_{\text{IF beat leakage}}$ and $\theta_{\text{IF leakage}}$, the following digital NCO can be generated.

$$\text{NCO}[n] = \cos\left(2\pi f_{\text{IF beat leakage}} n \frac{T_S}{Q} + \theta_{\text{IF leakage}}\right). \tag{16}$$

Then, the last down-conversion is done by multiplying $x[n]$ with NCO$[n]$. After the multiplication, the desired terms can be expressed as follows:

$$\begin{aligned} \psi[n] = &\underbrace{\frac{A_S A_L}{4}\cos\left(\varphi_{\text{IF leakage}}\left(n\frac{T_S}{Q}\right)\right)}_{\text{Leakage}} \\ &+ \underbrace{\frac{A_S A_{T,k}}{4}\sum_{k=1}^{K}\cos\left(2\pi f_{\text{beat targets, }k}\, n\frac{T_S}{Q} + \theta'_{\text{targets, }k} + \varphi_{\text{IF targets, }k}\left(n\frac{T_S}{Q}\right)\right)}_{\text{Targets}}. \end{aligned} \tag{17}$$

Then, the digital LPF and a decimation block can be added depending on the design.

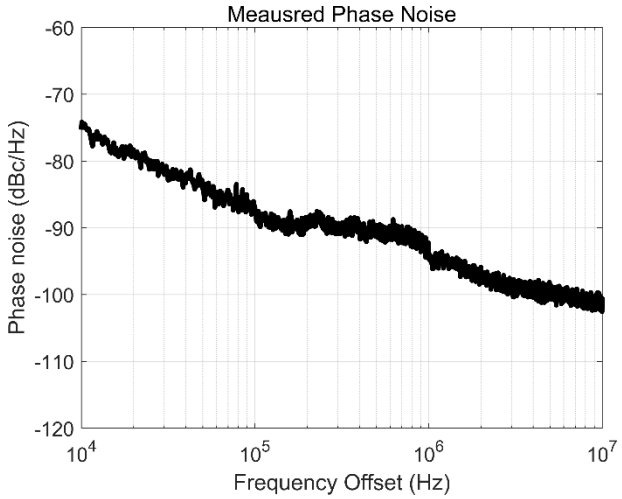

Fig. 5. Measured PSD of phase noise. It is the average of ten measurements with a spectrum analyzer, Agilent Technologies E4440A.

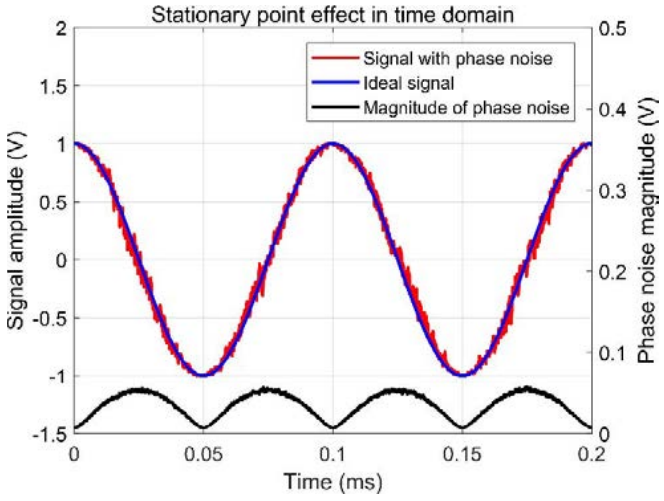

Fig. 6. Stationary point effect of phase noise in time domain. Results are the average of 1000 simulations.

IV. Simulations

In this section, the simulations are carried out to analyze the SPC technique and to predict the experiment results. A PSD of the phase noise from the measurement is usually used to get higher reliability of simulations [28], [37]. Also, an FMCW radar was simulated in the IF domain for the faster performance in [37]. Referring to these, in this paper, the PSD of the phase noise that is measured in the RX IF stage is used to enhance the reliability of the simulation. Based on this phase noise information as depicted in Fig. 5, all simulations were conducted in the digital IF domain.

A. Stationary Point Effect Analysis in Time domain

The explanations about the stationary points and the maximum slope points in Fig. 2 and Section II-B are verified by the simulations in the time domain. Fig. 6 shows a simple example. For this example, two sinusoidal signals whose frequencies are 10 kHz and amplitudes are 1 were created

TABLE I
PARAMETERS OF HETERODYNE FMCW RADAR FOR SIMULATION/EXPERIMENT

Parameters	Values
Sweep period (T)	880 us
Desired digital bandwidth	1.25 MHz
Minimum available sampling frequency (F_S)	2.5 MHz
Oversampling factor (Q)	4
Oversampling frequency (QF_S)	10 MHz
# of samples in a chirp	8800
# of samples after discarding early part in a chirp	8192
IF carrier frequency ($f_{IF\ carrier}$)	2.5 MHz
Window	Hann
$NFFT$ for finding out $f_{IF\ beat\ leakage}$ and $\theta_{IF\ leakage}$	2^{20}
Desired maximum detectable range	1100 m
Apparent range resolution	1.074 m

by the sampling rate of 10 MHz. One includes the phase noise, and the other is just an ideal signal. The phase noise that is expressed as the voltage noise can be extracted by subtracting the ideal signal from the signal with the phase noise. We added the magnitude of the extracted phase noise on the graph in Fig. 6. As shown in Fig. 6, the magnitude of the phase noise approaches the local maximum as the phase goes to the maximum slope points and becomes the local minimum as the phase goes to the stationary points. The SPC technique makes good use of these properties. By concentrating the phase noise of the leakage on the stationary point, the SPC technique significantly mitigates the magnitude of it.

B. Performance Analysis of SPC Technique

Before the practical simulation to detect targets, we simulate in case the only the leakage signal exists to evaluate how the SPC technique mitigates the noise floor in the power spectrum. Provided the theory is properly realized, the magnitude of the phase noise of the leakage decrease and so does the noise floor. The parameters of the heterodyne FMCW radar are listed in Table I. In order to compare the experiment results with the simulation results, the same parameters were used in the simulations. For the value of NFFT, larger values yield more accurate $f_{\text{IF beat leakage}}$ and $\theta_{\text{IF leakage}}$. However, the excessive NFFT values cause an overload for the computation. In this paper, NFFT value of 2^{20} is used. This gives the FFT resolution of 9.54 Hz, based on the oversampling frequency. Thus, the maximum error of $f_{\text{IF beat leakage}}$ due to the FFT resolution is about 4.77 Hz. In this paper, $f_{\text{IF carrier}}$ is 2.5 MHz. When $f_{\text{beat leakage}}$ is 10 kHz, $f_{\text{IF beat leakage}}$ is 2.51 MHz. The error ratio of $f_{\text{IF beat leakage}}$ due to the FFT resolution is only about 0.00019%. Therefore, the zero-padding that we used provides a sufficient FFT resolution to find out accurate values of $f_{\text{IF beat leakage}}$ and $\theta_{\text{IF leakage}}$. An Intel N3060 CPU and a 4 GB RAM yields only about 0.095 s of the computation time.

Fig. 7 shows the performance of the SPC technique in the power spectrum. For a clear comparison, we took an average on the power spectra from 100 chirps, which reduced the variance of the noise floor. The entire power spectrum is shifted to

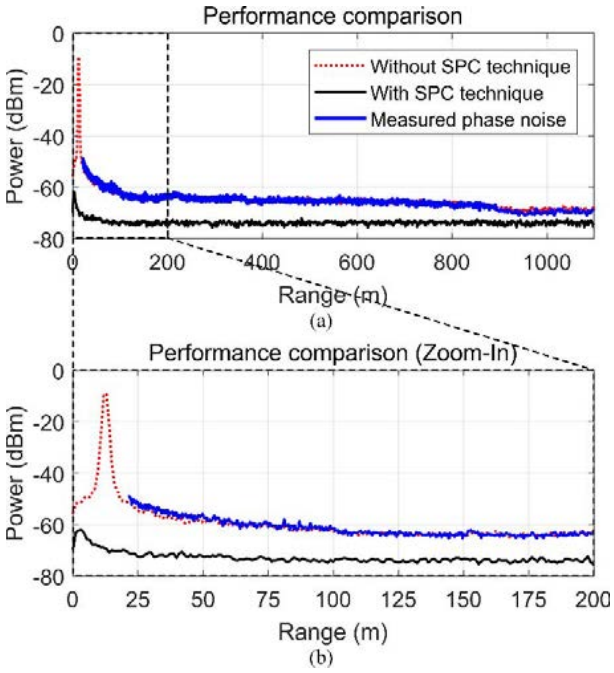

Fig. 7. Simulation results of leakage mitigation. (a) Performance comparison of the power spectrum. (b) Zoomed-in version of (a). The results are the average of 100 power spectra.

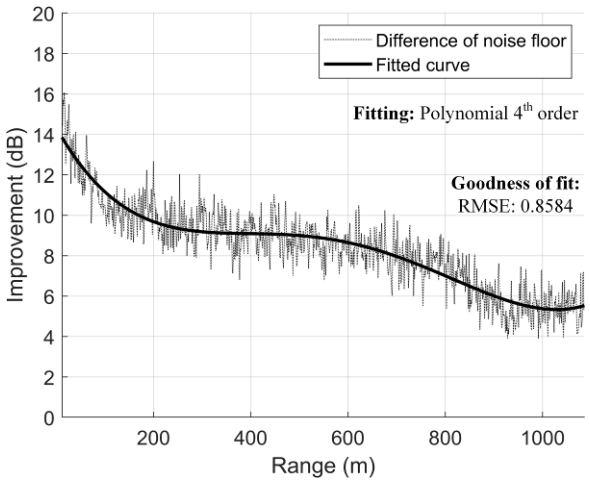

Fig. 8. Degree of improvement in simulation.

the left by the beat frequency of the leakage because the SPC technique involves the subtraction of the beat frequency. The remarkable mitigation of the leakage is apparent in Fig. 7. As depicted in Fig. 7, the measured phase noise is in concordance with the noise floor. Thus, the simulation accurately reflects the measured phase noise. From the results, we can expect that the proposed SPC technique will mitigate the high-noise floor caused by the phase noise of the leakage. The performance improvement of the SPC technique is shown clearly in Fig. 8. In Fig. 8, the graph displays the difference of noise floors when subtracted after the alignment of the two power spectra. In order to access the improvement, a fit curve is overlaid. The maximum and the minimum degrees of the improvement are predicted to be around 13.8 and 5.3 dB, respectively.

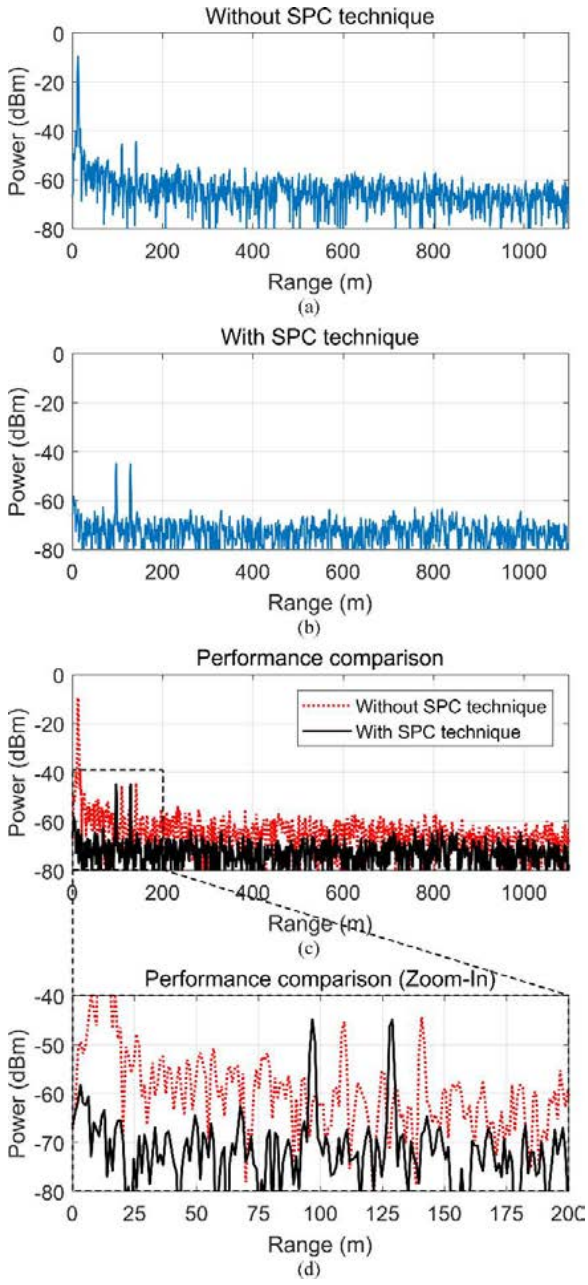

Fig. 9. Simulation results of target detection with leakage mitigation. (a) and (b) Power spectra from the common method without the SPC technique and from the SPC technique. (c) Comparison of the power spectrum. (d) Zoomed-in version of (c).

C. Target Detection With SPC Technique

The target detection was simulated referring the experiment plans in Section VI. We consider the real-time target detection, which is the practical. Thus, we show the results using only one chirp without a zero-padding or averaging the power spectra. Signals from two targets were added for the simulation. An adequate signal power was set to evaluate the clear improvement of the SNR. Provided the proposed theories are correct, the SNRs of the target signals will increase as the noise floor decreases. The expected results are depicted in Fig. 9. The SNR of the target signals significantly increases by the SPC technique. Because of the same reason that we mentioned in Section IV-B, the power spectrum from the SPC technique is shifted to the left. Also, as explained in Section II-B, there is little influence on the power of the target signals by the changed constant phases from the SPC technique.

TABLE II
SPECIFICATIONS OF THE *Ku*-BAND HETERODYNE FMCW RADAR

Property	Value	Units
Operating frequency	14.35-14.50	GHz
Transmit power	30	dBm
Antenna gain	16	dBi
Sweep bandwidth	150	MHz
Range resolution	1	m

V. RADAR SYSTEM

A *Ku*-band heterodyne FMCW radar was used to verify the performance of the proposed SPC technique. The *Ku*-band heterodyne FMCW radar has been continuously upgraded for the purpose of the drone detection by Microwave & Antenna Laboratory in Korea Advanced Institute of Science and Technology (KAIST). The specifications of the radar are listed in Table II.

Fig. 10 shows a block diagram of the radar. The radar mostly consists of the baseband (BB) and IF stages, a block up converter, a low-noise block, and antennas. The BB and the IF stages are located together in a metal case. Analog Device AD9854, a direct digital synthesizer, is used to generate the LFM signal with a high linearity. Corrugated conical horn antennas were used for the TX and RX. They provide a high efficiency and form a rotationally symmetric beam pattern [38]. The radar includes a software defined radio, Ettus USRP N210. We used USRP N210 to oversample IF beat signals and position $f_{\text{IF carrier}}$ for the experiments. The remaining procedures of the proposed technique after the oversampling were done using MATLAB in a mini-PC.

VI. EXPERIMENTS, RESULTS, AND DISCUSSION

A. Experiments

Radar setup for the experiments is shown in Fig. 11. The quasi-monostatic configuration was chosen. The distance between two antennas was 25 cm. The antennas were set to look up at the sky and the system was installed at the rooftop of a building in KAIST. These are conditions used in order to have the received signals contain only the leakage and the reflected waves by the desired targets. We used the small drones, DJI Spark and DJI Inspire I for the targets. We performed two experiments, *Experiment A* and *Experiment B*, to demonstrate the proposed SPC technique.

In *Experiment A*, we focused on observing the reduced noise floor, which is directly related to the phase noise of the leakage signal. We therefore measured the signal in a situation with no target introduced to the radar, receiving only the leakage signal. By doing so, we can clearly see the noise floor comparison between the SPC technique and the common method. This experiment demonstrates the simulation analysis

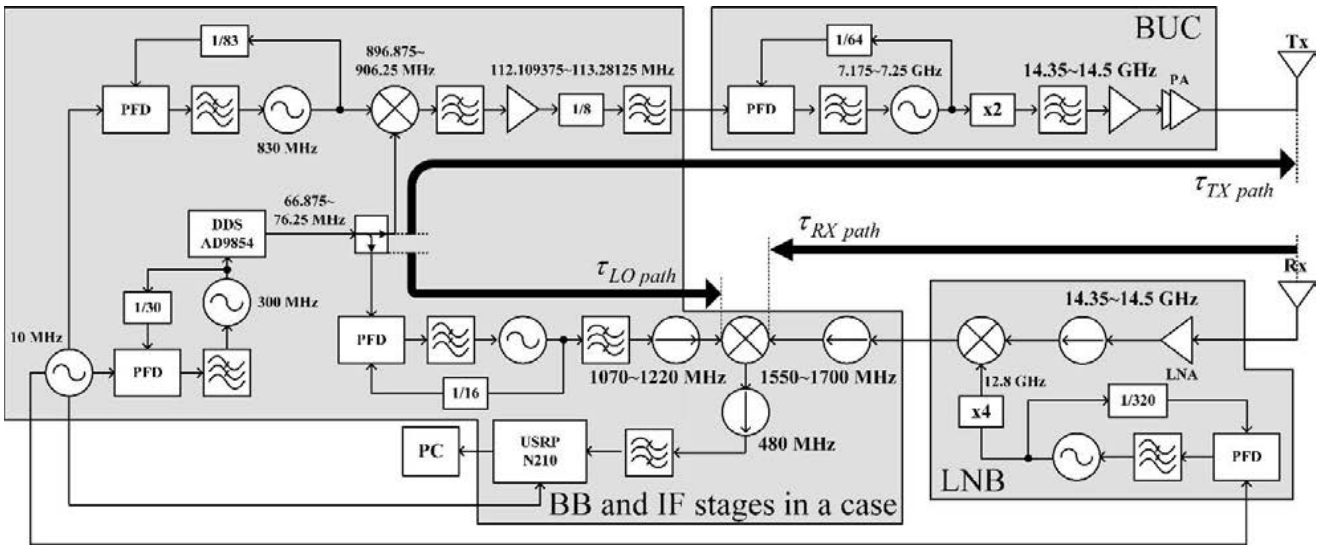

Fig. 10. Block diagram of the *Ku*-band heterodyne FMCW radar system.

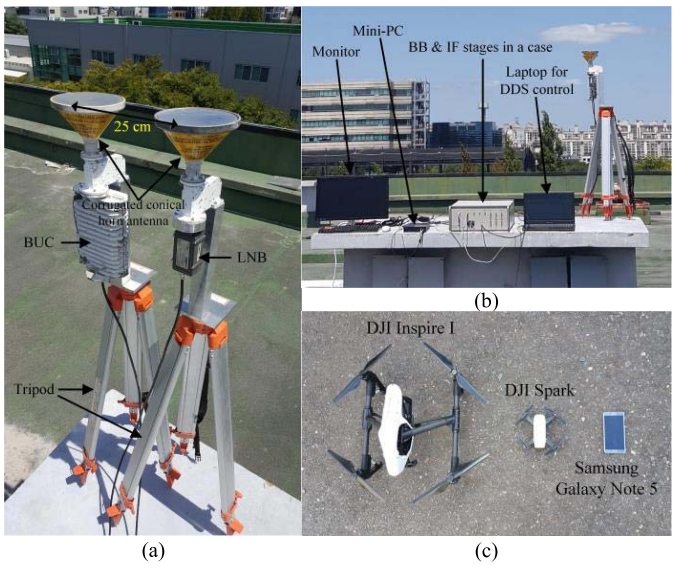

Fig. 11. Radar setup and targets. (a) RF front-end. (b) Other sections of the radar. The small drones, DJI Spark, and DJI Inspire I are shown in (c).

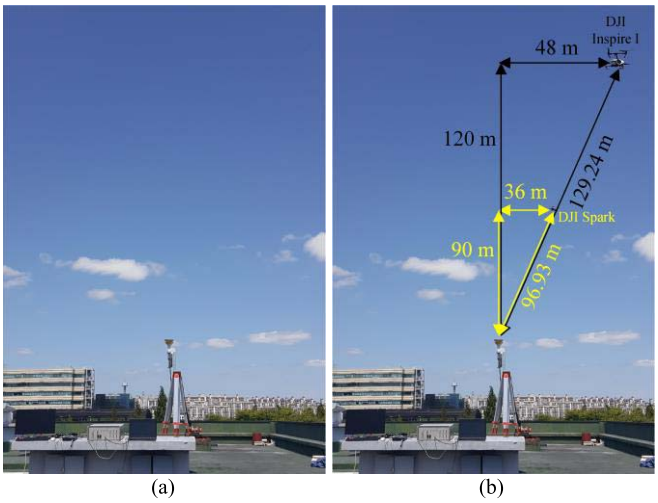

Fig. 12. Experiment scenarios. (a) *Experiment A*. (b) *Experiment B*.

in Section IV-B. Fig. 12(a) shows the arrangement of the experiment.

In *Experiment B*, we intentionally placed the small drones at a slightly askew direction from the boresight. This way, with the SPC technique, shows that it is possible to effectively detect the targets even though the received signals are weak since they are out of the boresight. For instance, we can detect the drones when they try to invade using relatively weak beam area to break defenses. The GPS information was used for the precise positioning of the drones. The actual distances of the small drones were measured by GPS module inside the drones. The intrinsic error of the GPS module inside DJI Inspire I is within ± 0.5 m vertically and within ± 2.5 m horizontally, and that of the GPS module in DJI Spark is within ± 0.5 m vertically and within ± 1.5 m horizontally. This experiment demonstrates the simulation analysis in Section IV-C. Fig. 12(b) shows the configuration of *Experiment B*.

B. Results and Discussion on Experiment A

The results of *Experiment A* are shown in Figs. 13 and 14. As we did in the simulations, we took an average on the power spectra from 100 chirps for the clear comparison. In Fig. 13, the noise floor is well matched with the measured phase noise. Also, Fig. 13 shows a noticeable improvement in the mitigation of the leakage. Therefore, it is verified that the proposed SPC technique reduces the noise floor caused by the phase noise of the leakage. In Fig. 14, the difference of noise floor is the subtraction of the two resulting power spectra in Fig. 13(a). During the subtraction, the two power spectra were aligned, and the leakage peak is not considered. The maximum and the minimum degrees of the improvement are about 10.5 and 5.2 dB, respectively.

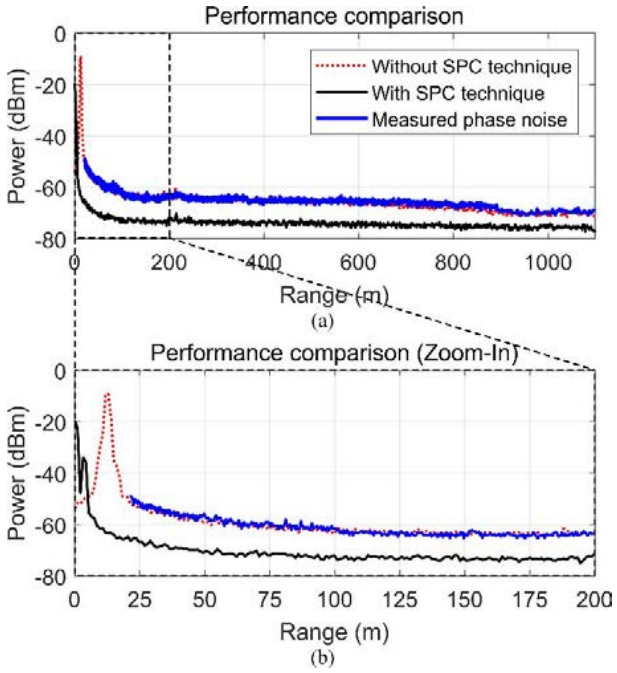

Fig. 13. Results of *Experiment A*. (a) Performance comparison of the power spectrum. (b) Zoomed-in version of (a). The results are the average of 100 power spectra.

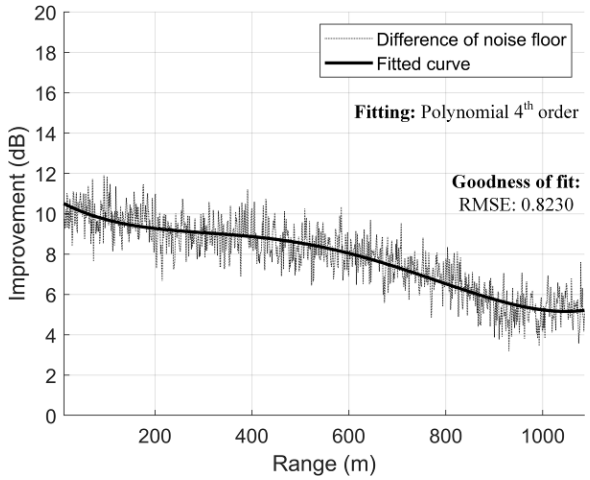

Fig. 14. Degree of improvement in *Experiment A*.

Fig. 15 gives the clear comparison between the simulations and the experiments. The difference of the improvement is within 1 dB over the range domain. However, in the near distances, the difference is widened up to 3.3 dB. The reason of this can be explained by comparing the simulation results, Fig. 7(b) and the experiment result, Fig. 13(b). While the results in Fig. 7(b) present a complete leakage mitigation from a single dominant leakage assumption, some components near dc are observed in Fig. 13(b). Also, the powers of the components are less than the power of the leakage of the dotted line in Fig. 13(b). Therefore, the components near dc in the experiment result, Fig. 13(b), are not the dominant leakage but other minor leakages from minor leakage paths. Because of these other minor leakages, the expected improvement

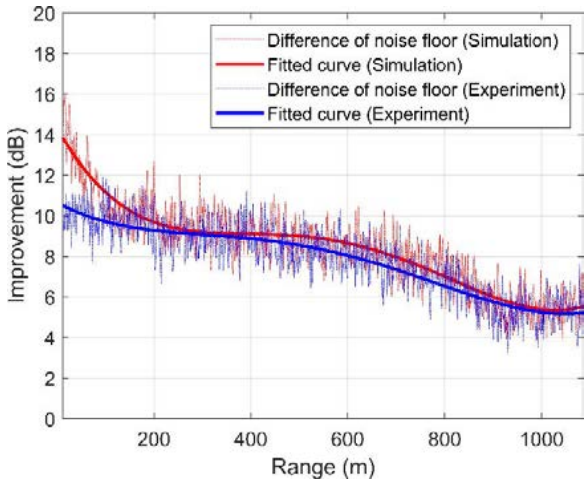

Fig. 15. Comparison between simulation and experiment results of improvement performance.

results from the simulations deviate that of the experiment in the near-distances. Although the minor leakages exist, however, the proposed SPC technique definitely mitigates the dominant leakage as we aimed in this paper. This fact leads to the significantly improved power spectrum. In addition, these results and discussion show a potential that the SPC technique can be used for a complex-environments-based radar applications such as indoor detection and automotive radars. In light of the results, the SPC technique could mitigate the most dominant one of nearby-clutter signals, which makes the worst noise floor in the complex environment.

C. Results and Discussion on Experiment B

Fig. 16 shows the results of *Experiment B*. Only one chirp was used for the results to perform the real-time target detection that is practical. Thus, the averaging and the zero-padding were not applied. As shown in Fig. 16, the SNRs of the target signals are significantly increased. Based on these results, we can be sure that the maximum detectable distance for the small drones is increased by the SPC technique. When we detect the drones that are moving away from the radar, the drones disappear earlier in case of the common method based radar than in case of the SPC technique based radar. In other words, when we try to detect invading drones for terrorisms, the SPC technique-based radar will detect the drones earlier than the common method based radar.

The distance information measured in Fig. 16(b) is quite accurate when it is compared with the actual distance in Fig. 12(b). For the common method without the SPC technique, the received signals from the targets not only have the delay due to the target distance but also the total internal delay in the radar. This total internal delay corresponds to the beat frequency of the dominant leakage. On the other hand, for the SPC technique, only the beat frequencies of the targets remain in the target beat signals, because the beat frequency of the dominant leakage is deleted in the target beat signals. This results in the shift of the power spectrum to the left and provides more precise distance information than the common method. In Fig. 16(d), it is shown that the powers of the target

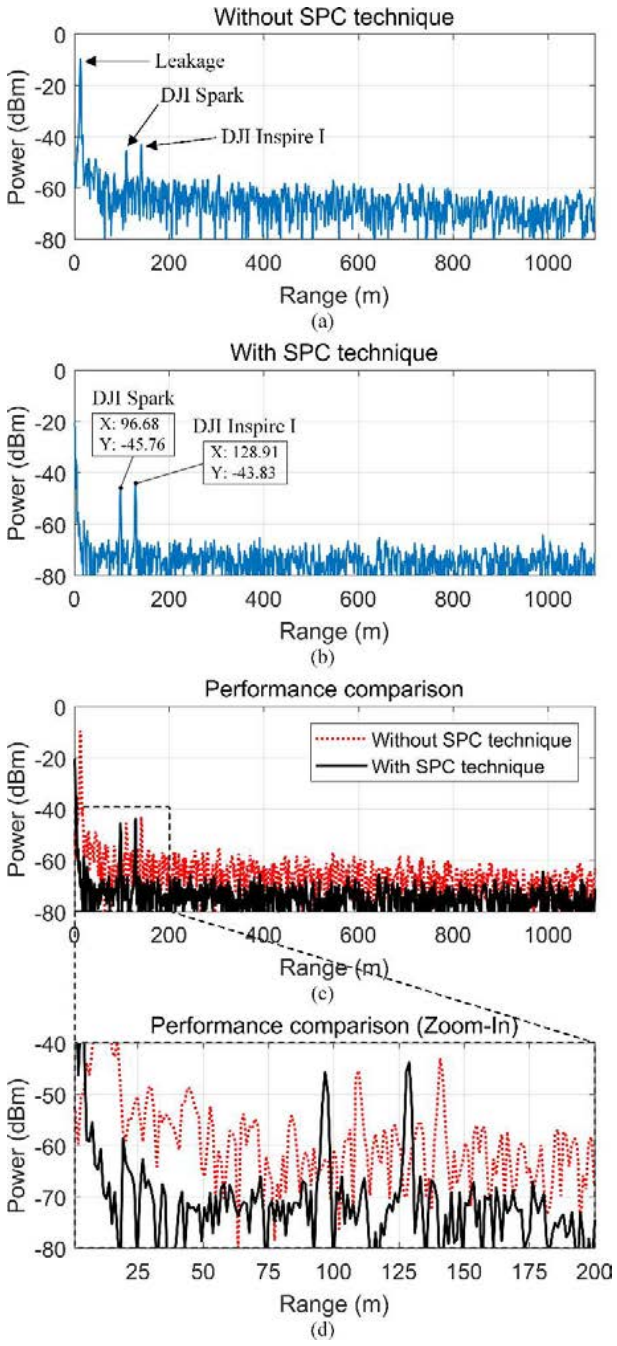

Fig. 16. Results of *Experiment B*. (a) and (b) Power spectra from the common method without the SPC technique and from the SPC technique. (c) Comparison of the power spectrum. (d) Zoomed-in version of (c).

beat signals remain the same. This verifies the theories and the simulation results, which insist that there is little influence even though the constant phases in the target beat signals are changed by the SPC technique.

VII. Conclusion

The SPC technique to mitigate the dominant leakage in the heterodyne FMCW radar for the small drone detection has been explained and demonstrated in detail with the theories, the simulations, and the experiments. Unlike the major trend in this research field, the proposed technique suggests a new approach to mitigate the leakage. Also, the proposed technique can be realized using DSP without any additional hardware parts. The results verify that the proposed technique significantly increases the SNR of the targets by decreasing the noise floor due to the phase noise of the dominant leakage. Additionally, the proposed technique provides accurate distance information of the targets.

References

[1] U. Fuchs and W. Sieprath, "Advanced ground-based ESCAN radars," in *IEEE MTT-S Int. Microw. Symp. Dig.*, Jun. 2005, pp. 1461–1464.

[2] J. Martinez, D. Kopyto, M. Schütz, and M. Vossiek, "Convolutional neural network assisted detection and localization of UAVs with a narrowband multi-site radar," in *IEEE MTT-S Int. Microw. Symp. Dig.*, Munich, Germany, Apr. 2018, pp. 1–4.

[3] Y. Wang, T. Phelps, K. Kibaroglu, M. Sayginer, Q. Ma, and G. M. Rebeiz, "28 GHz 5G-based phased-arrays for UAV detection and automotive traffic-monitoring radars," in *IEEE MTT-S Int. Microw. Symp. Dig.*, Philadelphia, PA, USA, Jun. 2018, pp. 895–898.

[4] T. Multerer *et al.*, "Low-cost jamming system against small drones using a 3D MIMO radar based tracking," in *Proc. 14th Eur. Radar Conf.*, Nuremberg, Germany, 2017, pp. 299–302.

[5] S. Park and S.-O. Park, "Configuration of an X-band FMCW radar targeted for drone detection," in *Proc. Int. Symp. Antennas Propag.*, Phuket, Thailand, 2017, pp. 1–2.

[6] K. Wu, K. Wang, and X. Liu, "A mini radar system for low altitude targets detection," in *Proc. 10th Int. Congr. Image Signal Process., Biomed. Eng. Inform.*, 2017, pp. 1–5.

[7] D.-H. Shin, D.-H. Jung, D.-C. Kim, J.-W. Ham, and S.-O. Park, "A distributed FMCW radar system based on fiber-optic links for small drone detection," *IEEE Trans. Instrum. Meas.*, vol. 66, no. 2, pp. 340–347, Feb. 2017.

[8] J. Drozdowicz *et al.*, "35 GHz FMCW drone detection system," in *Proc. 17th Int. Radar Symp.*, 2016, pp. 1–4.

[9] N. J. Kinzie, "Ultra-wideband pulse Doppler radar for short-range targets," Ph.D. dissertation, Dept. Elect. Comput. Eng., Univ. Colorado Boulder, Boulder, CO, USA, 2008.

[10] B. Razavi, "Design considerations for direct-conversion receivers," *IEEE Trans. Circuits Syst. II, Analog Digit. Signal Process.*, vol. 44, no. 6, pp. 428–435, Jun. 1997.

[11] J.-S. Suh, L. Minz, D.-H. Jung, H.-S. Kang, J.-W. Ham, and S.-O. Park, "Drone-based external calibration of a fully synchronized ku-band heterodyne FMCW radar," *IEEE Trans. Instrum. Meas.*, vol. 66, no. 8, pp. 2189–2197, Aug. 2017.

[12] A. Anghel, G. Vasile, R. Cacoveanu, C. Ioana, and S. Ciochina, "Short-range FMCW X-band radar platform for millimetric displacements measurement," in *Proc. IEEE Int. Geosci. Remote Sens. Symp.*, Jul. 2013, pp. 1111–1114.

[13] A. Anghel, G. Vasile, R. Cacoveanu, C. Ioana, and S. Ciochina, "Short-range wideband FMCW radar for millimetric displacement measurements," *IEEE Trans. Geosci. Remote Sens.*, vol. 52, no. 9, pp. 5633–5642, Sep. 2014.

[14] B. Boukari, E. Moldovan, S. Affes, K. Wu, R. G. Bosisio, and S. O. Tatu, "A heterodyne six-port FMCW radar sensor architecture based on beat signal phase slope techniques," *Prog. Electromagn. Res.*, vol. 93, pp. 307–322, Jul. 2009.

[15] K. Lin, Y. E. Wang, C.-K. Pao, and Y.-C. Shih, "A *Ka*-band FMCW radar front-end with adaptive leakage cancellation," *IEEE Trans. Microw. Theory Techn.*, vol. 54, no. 12, pp. 4041–4048, Dec. 2006.

[16] P. D. L. Beasley, A. G. Stove, B. J. Reits, and B. As, "Solving the problems of a single antenna frequency modulated CW radar," in *Proc. IEEE Int. Conf. Radar*, Arlington, VA, USA, May 1990, pp. 391–395.

[17] K. Lin, R. H. Messerian, and Y. Wang, "A digital leakage cancellation scheme for monostatic FMCW radar," in *IEEE MTT-S Int. Microw. Symp. Dig.*, vol. 2, Jun. 2004, pp. 747–750.

[18] K. Lin and Y. E. Wang, "Transmitter noise cancellation in monostatic FMCW radar," in *IEEE MTT-S Int. Microw. Symp. Dig.*, Jun. 2006, pp. 1406–1409.

[19] M. Yuehong, L. Qiusheng, and Z. Xiaolin, "Research on carrier leakage cancellation technology of FMCW system," in *Proc. 18th Int. Conf. Adv. Commun. Technol.*, Pyeongchang, South Korea, 2016, pp. 7–9.

[20] J.-G. Kim, S. Ko, S. Jeon, J.-W. Park, and S. Hong, "Balanced topology to cancel Tx leakage in CW radar," *IEEE Microw. Wireless Compon. Lett.*, vol. 14, no. 9, pp. 443–445, Sep. 2004.
[21] C. Kim *et al.*, "Tx leakage cancellers for 24 GHz and 77 GHz vehicular radar applications," in *IEEE MTT-S Int. Microw. Symp. Dig.*, Jun. 2006, pp. 1402–1405.
[22] C.-Y. Kim, J.-G. Kim, and S. Hong, "A quadrature radar topology with Tx leakage canceller for 24-GHz radar applications," *IEEE Trans. Microw. Theory Techn.*, vol. 55, no. 7, pp. 1438–1444, Jul. 2007.
[23] M. Nalezinski, M. Vossiek, and P. Heide, "Novel 24 GHz FMCW front-end with 2.45 GHz SAW reference path for high-precision distance measurements," in *IEEE MTT-S Int. Microw. Symp. Dig.*, Jun. 1997, pp. 185–188.
[24] R. Feger, C. Wagner, and A. Stelzer, "A W-band heterodyne FMCW radar based on TX IQ-modulation," *Frequenz*, vol. 65, nos. 7–8, pp. 183–191, Aug. 2011.
[25] R. Feger, E. Kolmhofer, F. Starzer, F. Wiesinger, S. Scheiblhofer, and A. Stelzer, "A heterodyne 77-GHz FMCW radar with offset PLL frequency stabilization," in *Proc. IEEE Top. Conf. Wireless Sensors Sensor Netw.*, Phoenix, AZ, USA, Jan. 2011, pp. 9–12.
[26] M.-T. Dao, D.-H. Shin, Y.-T. Im, and S.-O. Park, "A two sweeping VCO source for heterodyne FMCW radar," *IEEE Trans. Instrum. Meas.*, vol. 62, no. 1, pp. 230–239, Jan. 2013.
[27] R. Feger, H. J. Ng, C. Pfeffer, and A. Stelzer, "A Delta–Sigma modulator-based heterodyne FMCW radar for short-range applications," *Int. J. Microw. Wireless Technol.*, vol. 6, pp. 379–387, Jun. 2014.
[28] A. Melzer, A. Onic, F. Starzer, and M. Huemer, "Short-range leakage cancelation in FMCW radar transceivers using an artificial on-chip target," *IEEE J. Sel. Topics Signal Process.*, vol. 9, no. 8, pp. 1650–1660, Dec. 2015.
[29] A. Melzer, F. Starzer, H. Jäger, and M. Huemer, "On-chip delay line for extraction of decorrelated phase noise in FMCW radar transceiver MMICs," in *Proc. 23rd Austrian Workshop Microelectron.*, Vienna, Austria, 2015, pp. 31–35.
[30] A. Melzer, F. Starzer, H. Jäger, and M. Huemer, "Real-time mitigation of short-range leakage in automotive FMCW radar transceivers," *IEEE Trans. Circuits Syst. II, Exp. Briefs*, vol. 64, no. 7, pp. 847–851, Jul. 2017.
[31] A. Melzer, M. Huemer, and A. Onic, "Novel mixed-signal based short-range leakage canceler for FMCW radar transceiver MMICs," in *Proc. IEEE Int. Symp. Circuits Syst.*, Baltimore, MD, USA, May 2017, pp. 1–4.
[32] J. Park and S.-O. Park, "A down-conversion method for attenuation of leakage signal in FMCW radar," in *Proc. Int. Symp. Antennas Propag.*, Phuket, Thailand, 2017, pp. 1–2.
[33] M. C. Budge, Jr., and M. P. Burt, "Range correlation effects in radars," in *Proc. Rec. IEEE Nat. Radar Conf.*, Lynnfield, MA, USA, Apr. 1993, pp. 212–216.
[34] B. Razavi, *RF Microelectronics*, 2nd ed. Upper Saddle River, NJ, USA: Prentice-Hall, 2012.
[35] A. V. Oppenheim and R. W. Schafer, *Discrete-Time Signal Processing*, 3rd ed. Upper Saddle River, NJ, USA: Prentice-Hall, 2010.
[36] R. G. Lyons, *Understanding Digital Signal Processing*, 3rd ed. Upper Saddle River, NJ, USA: Prentice-Hall, 2010.
[37] M. Gerstmair, A. Melzer, A. Onic, R. Stuhlberger, and M. Huemer, "Highly efficient environment for FMCW radar phase noise simulations in IF domain," *IEEE Trans. Circuits Syst. II, Exp. Briefs*, vol. 65, no. 5, pp. 582–586, May 2018.
[38] C. A. Balanis, *Antenna Theory: Analysis and Design*, 3rd ed. Hoboken, NJ, USA: Wiley, 2005.

Junhyeong Park (GS'18) received the B.S. and M.S. degrees in electrical engineering from the Korea Advanced Institute of Science and Technology, Daejeon, South Korea, in 2015 and 2017, where he is currently pursuing the Ph.D. degree in electrical engineering.

His current research interests include frequency modulated continuous-wave radar system for drone detection, radar target classification, and radar signal processing.

Seungwoon Park received the B.S. and M.S. degrees in electrical engineering from the Korea Advanced Institute of Science and Technology (KAIST), Daejeon, South Korea, in 2016 and 2018, where he is currently pursuing the Ph.D. degree in electrical engineering.

His current research interests include frequency-modulated continuous-wave radar system for drone detection.

Do-Hoon Kim received the B.S. degree in electrical engineering from Yonsei University, Seoul, South Korea, in 2017. He is currently pursuing the M.S. degree in electrical engineering at the Korea Advanced Institute of Science and Technology, Daejeon, South Korea.

His current research interest include radar signal processing.

Seong-Ook Park (M'05–SM'11) was born in Yeongcheon, South Korea, in 1964. He received the B.S. degree in electrical engineering from Kyung-Pook National University, Daegu, South Korea, in 1987, the M.S. degree in electrical engineering from the Korea Advanced Institute of Science and Technology, Daejeon, South Korea, in 1989, and the Ph.D. degree in electrical engineering from Arizona State University, Tempe, AZ, USA, in 1997.

From 1989 to 1993, he was a Research Engineer with Korea Telecom, Daejeon, where he was involved in microwave systems and networks. He then was with the Telecommunication Research Center, Arizona State University, until 1997. Since 1997, he has been a Professor with the Korea Advanced Institute of Science and Technology. His current research interests include antenna, radar system, and analytical and numerical techniques in the area of electromagnetics.

Dr. Park is a member of Pi Kappa Phi.